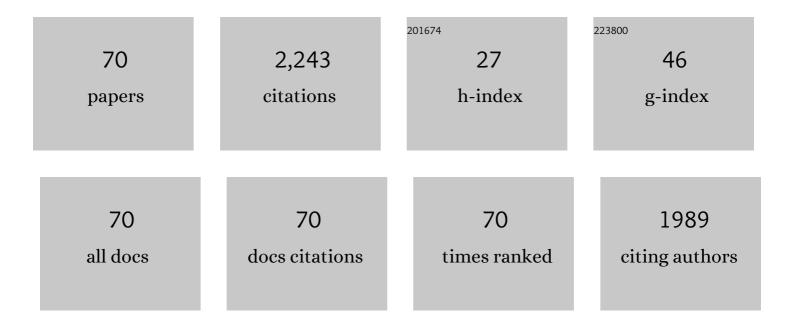
Xiaodong Li

List of Publications by Year in descending order

Source: https://exaly.com/author-pdf/1574260/publications.pdf Version: 2024-02-01



XIAODONC LI

#	Article	IF	CITATIONS
1	Superresolution Land Cover Mapping Using a Generative Adversarial Network. IEEE Geoscience and Remote Sensing Letters, 2022, 19, 1-5.	3.1	6
2	Spatiotemporal Reflectance Fusion Using a Generative Adversarial Network. IEEE Transactions on Geoscience and Remote Sensing, 2022, 60, 1-15.	6.3	7
3	RFSDAF: A New Spatiotemporal Fusion Method Robust to Registration Errors. IEEE Transactions on Geoscience and Remote Sensing, 2022, 60, 1-18.	6.3	2
4	A Cascaded Spectral–Spatial CNN Model for Super-Resolution River Mapping With MODIS Imagery. IEEE Transactions on Geoscience and Remote Sensing, 2022, 60, 1-13.	6.3	6
5	AHSWFM: Automated and Hierarchical Surface Water Fraction Mapping for Small Water Bodies Using Sentinel-2 Images. Remote Sensing, 2022, 14, 1615.	4.0	7
6	Destruction of gasification tar over Ni catalysts in a modified rotating gliding arc plasma reactor: Effect of catalyst position and nickel loading. Fuel, 2021, 289, 119742.	6.4	13
7	Informing action for United Nations SDG target 8.7 and interdependent SDGs: Examining modern slavery from space. Humanities and Social Sciences Communications, 2021, 8, .	2.9	4
8	Estimating subpixel turbulent heat flux over leads from MODIS thermal infrared imagery with deep learning. Cryosphere, 2021, 15, 2835-2856.	3.9	2
9	Spatiotemporal Continuous Impervious Surface Mapping by Fusion of Landsat Time Series Data and Google Earth Imagery. Remote Sensing, 2021, 13, 2409.	4.0	8
10	Tracking small-scale tropical forest disturbances: Fusing the Landsat and Sentinel-2 data record. Remote Sensing of Environment, 2021, 261, 112470.	11.0	32
11	Object-Based Area-to-Point Regression Kriging for Pansharpening. IEEE Transactions on Geoscience and Remote Sensing, 2021, 59, 8599-8614.	6.3	13
12	Monitoring high spatiotemporal water dynamics by fusing MODIS, Landsat, water occurrence data and DEM. Remote Sensing of Environment, 2021, 265, 112680.	11.0	33
13	Mapping water bodies under cloud cover using remotely sensed optical images and a spatiotemporal dependence model. International Journal of Applied Earth Observation and Geoinformation, 2021, 103, 102470.	2.8	9
14	SFSDAF: An enhanced FSDAF that incorporates sub-pixel class fraction change information for spatio-temporal image fusion. Remote Sensing of Environment, 2020, 237, 111537.	11.0	86
15	Monitoring surface water area variations of reservoirs using daily MODIS images by exploring sub-pixel information. ISPRS Journal of Photogrammetry and Remote Sensing, 2020, 168, 141-152.	11.1	36
16	Spatio-Temporal Sub-Pixel Land Cover Mapping of Remote Sensing Imagery Using Spatial Distribution Information From Same-Class Pixels. Remote Sensing, 2020, 12, 503.	4.0	6
17	Urbanization effects on changes in the observed air temperatures during 1977–2014 in China. International Journal of Climatology, 2019, 39, 251-265.	3.5	15
18	Measuring River Wetted Width From Remotely Sensed Imagery at the Subpixel Scale With a Deep Convolutional Neural Network. Water Resources Research, 2019, 55, 5631-5649.	4.2	51

XIAODONG LI

#	Article	IF	CITATIONS
19	Permanent disappearance and seasonal fluctuation of urban lake area in Wuhan, China monitored with long time series remotely sensed images from 1987 to 2016. International Journal of Remote Sensing, 2019, 40, 8484-8505.	2.9	11
20	Spatial–Temporal Super-Resolution Land Cover Mapping With a Local Spatial–Temporal Dependence Model. IEEE Transactions on Geoscience and Remote Sensing, 2019, 57, 4951-4966.	6.3	11
21	Optimal Endmember-Based Super-Resolution Land Cover Mapping. IEEE Geoscience and Remote Sensing Letters, 2019, 16, 1279-1283.	3.1	6
22	Earth Observation and Machine Learning to Meet Sustainable Development Goal 8.7: Mapping Sites Associated with Slavery from Space. Remote Sensing, 2019, 11, 266.	4.0	32
23	Mapping annual forest cover by fusing PALSAR/PALSAR-2 and MODIS NDVI during 2007–2016. Remote Sensing of Environment, 2019, 224, 74-91.	11.0	52
24	Aging brick kilns in the asian brick belt using a long time series of Landsat sensor data to inform the study of modern day slavery. , 2019, , .		3
25	Spatio-Temporal Super-Resolution Land Cover Mapping Based on Fuzzy C-Means Clustering. Remote Sensing, 2018, 10, 1212.	4.0	11
26	Spatial-temporal fraction map fusion with multi-scale remotely sensed images. Remote Sensing of Environment, 2018, 213, 162-181.	11.0	30
27	Urban Land Use Mapping by Combining Remote Sensing Imagery and Mobile Phone Positioning Data. Remote Sensing, 2018, 10, 446.	4.0	58
28	Spectral–Spatial Adaptive Area-to-Point Regression Kriging for MODIS Image Downscaling. IEEE Journal of Selected Topics in Applied Earth Observations and Remote Sensing, 2017, 10, 1883-1896.	4.9	11
29	Generating a series of fine spatial and temporal resolution land cover maps by fusing coarse spatial resolution remotely sensed images and fine spatial resolution land cover maps. Remote Sensing of Environment, 2017, 196, 293-311.	11.0	98
30	Updating Landsat-based forest cover maps with MODIS images using multiscale spectral-spatial-temporal superresolution mapping. International Journal of Applied Earth Observation and Geoinformation, 2017, 63, 129-142.	2.8	8
31	Learning-Based Spatial–Temporal Superresolution Mapping of Forest Cover With MODIS Images. IEEE Transactions on Geoscience and Remote Sensing, 2017, 55, 600-614.	6.3	26
32	Impervious Surface Change Mapping with an Uncertainty-Based Spatial-Temporal Consistency Model: A Case Study in Wuhan City Using Landsat Time-Series Datasets from 1987 to 2016. Remote Sensing, 2017, 9, 1148.	4.0	30
33	Monitoring Thermal Pollution in Rivers Downstream of Dams with Landsat ETM+ Thermal Infrared Images. Remote Sensing, 2017, 9, 1175.	4.0	38
34	Assessing a Temporal Change Strategy for Sub-Pixel Land Cover Change Mapping from Multi-Scale Remote Sensing Imagery. Remote Sensing, 2016, 8, 642.	4.0	11
35	Water Bodies' Mapping from Sentinel-2 Imagery with Modified Normalized Difference Water Index at 10-m Spatial Resolution Produced by Sharpening the SWIR Band. Remote Sensing, 2016, 8, 354.	4.0	486
36	Locally adaptive linear mixture model-based super-resolution land-cover mapping based on a structure tensor. International Journal of Remote Sensing, 2016, 37, 5802-5825.	2.9	3

XIAODONG LI

#	Article	IF	CITATIONS
37	An Iterative Interpolation Deconvolution Algorithm for Superresolution Land Cover Mapping. IEEE Transactions on Geoscience and Remote Sensing, 2016, 54, 7210-7222.	6.3	10
38	Land cover blending: A new framework to generate high spatial and temporal resolution land cover maps from remotely sensed images. , 2016, , .		0
39	Improving super-resolution mapping through combining multiple super-resolution land-cover maps. International Journal of Remote Sensing, 2016, 37, 2415-2432.	2.9	12
40	Learning-Based Superresolution Land Cover Mapping. IEEE Transactions on Geoscience and Remote Sensing, 2016, 54, 3794-3810.	6.3	23
41	A Superresolution Land-Cover Change Detection Method Using Remotely Sensed Images With Different Spatial Resolutions. IEEE Transactions on Geoscience and Remote Sensing, 2016, 54, 3822-3841.	6.3	34
42	Sub-pixel-scale Land Cover Map Updating by Integrating Change Detection and Sub-Pixel Mapping. Photogrammetric Engineering and Remote Sensing, 2015, 81, 59-67.	0.6	14
43	Spectral–spatial based sub-pixel mapping of remotely sensed imagery with multi-scale spatial dependence. International Journal of Remote Sensing, 2015, 36, 2831-2850.	2.9	15
44	Super-Resolution Land Cover Mapping Using Multiscale Self-Similarity Redundancy. IEEE Journal of Selected Topics in Applied Earth Observations and Remote Sensing, 2015, 8, 5130-5145.	4.9	13
45	Burned-Area Mapping at the Subpixel Scale With MODIS Images. IEEE Geoscience and Remote Sensing Letters, 2015, 12, 1963-1967.	3.1	23
46	Improvement of the Example-Regression-Based Super-Resolution Land Cover Mapping Algorithm. IEEE Geoscience and Remote Sensing Letters, 2015, 12, 1740-1744.	3.1	11
47	Super-Resolution Mapping of Forests With Bitemporal Different Spatial Resolution Images Based on the Spatial-Temporal Markov Random Field. IEEE Journal of Selected Topics in Applied Earth Observations and Remote Sensing, 2014, 7, 29-39.	4.9	44
48	Superresolution Land Cover Mapping With Multiscale Information by Fusing Local Smoothness Prior and Downscaled Coarse Fractions. IEEE Transactions on Geoscience and Remote Sensing, 2014, 52, 5677-5692.	6.3	24
49	Unsupervised Subpixel Mapping of Remotely Sensed Imagery Based on Fuzzy C-Means Clustering Approach. IEEE Geoscience and Remote Sensing Letters, 2014, 11, 1024-1028.	3.1	17
50	Spatially Adaptive Superresolution Land Cover Mapping With Multispectral and Panchromatic Images. IEEE Transactions on Geoscience and Remote Sensing, 2014, 52, 2810-2823.	6.3	32
51	Superresolution Mapping of Remotely Sensed Image Based on Hopfield Neural Network With Anisotropic Spatial Dependence Model. IEEE Geoscience and Remote Sensing Letters, 2014, 11, 1265-1269.	3.1	31
52	Post-processing of interpolation-based super-resolution mapping with morphological filtering and fraction refilling. International Journal of Remote Sensing, 2014, 35, 5251-5262.	2.9	9
53	Superresolution Land Cover Mapping Using Spatial Regularization. IEEE Transactions on Geoscience and Remote Sensing, 2014, 52, 4424-4439.	6.3	41
54	Example-Based Super-Resolution Land Cover Mapping Using Support Vector Regression. IEEE Journal of Selected Topics in Applied Earth Observations and Remote Sensing, 2014, 7, 1271-1283.	4.9	48

XIAODONG LI

#	Article	IF	CITATIONS
55	Super-Resolution Land Cover Mapping with Spatial–Temporal Dependence by Integrating a Former Fine Resolution Map. IEEE Journal of Selected Topics in Applied Earth Observations and Remote Sensing, 2014, 7, 1816-1825.	4.9	21
56	A spatial–temporal Hopfield neural network approach for super-resolution land cover mapping with multi-temporal different resolution remotely sensed images. ISPRS Journal of Photogrammetry and Remote Sensing, 2014, 93, 76-87.	11.1	45
57	Interpolation-based super-resolution land cover mapping. Remote Sensing Letters, 2013, 4, 629-638.	1.4	68
58	Sub-pixel mapping of remotely sensed imagery with hybrid intra- and inter-pixel dependence. International Journal of Remote Sensing, 2013, 34, 341-357.	2.9	58
59	Improving Neural Network Prediction Accuracy for PM ₁₀ Individual Air Quality Index Pollution Levels. Environmental Engineering Science, 2013, 30, 725-732.	1.6	23
60	Monitoring river discharge with remotely sensed imagery using river island area as an indicator. Journal of Applied Remote Sensing, 2012, 6, 063564-1.	1.3	18
61	Spatially adaptive smoothing parameter selection for Markov random field based sub-pixel mapping of remotely sensed images. International Journal of Remote Sensing, 2012, 33, 7886-7901.	2.9	40
62	Object-based sub-pixel mapping of buildings incorporating the prior shape information from remotely sensed imagery. International Journal of Applied Earth Observation and Geoinformation, 2012, 18, 283-292.	2.8	53
63	Super-resolution mapping based on the supervised fuzzy <i>c</i> -means approach. Remote Sensing Letters, 2012, 3, 501-510.	1.4	25
64	Subpixel Land Cover Mapping by Integrating Spectral and Spatial Information of Remotely Sensed Imagery. IEEE Geoscience and Remote Sensing Letters, 2012, 9, 408-412.	3.1	46
65	Artificial Neural Network Models for Daily PM ₁₀ Air Pollution Index Prediction in the Urban Area of Wuhan, China. Environmental Engineering Science, 2011, 28, 357-363.	1.6	33
66	Using a sub-pixel mapping model to improve the accuracy of landscape pattern indices. Ecological Indicators, 2011, 11, 1160-1170.	6.3	39
67	Land Cover Change Mapping at the Subpixel Scale With Different Spatial-Resolution Remotely Sensed Imagery. IEEE Geoscience and Remote Sensing Letters, 2011, 8, 182-186.	3.1	95
68	Variations of PM10 concentrations in Wuhan, China. Environmental Monitoring and Assessment, 2011, 176, 259-271.	2.7	17
69	Characterizing sub-pixel landscape patterns from remotely sensed imagery with sub-pixel mapping methods. , 2010, , .		0

Footprint of Yangxin County: A Time Series for 1999-2006. , 2009, , .